Advanced Ceramics Progress: Vol. 7, No. 4, (Autumn 2021) 52-58

Materials and Energy Research Center
MERC

Contents lists available at ACERP

Advanced Ceramics Progress

Journal Homepage: www.acerp.ir

Original Research Article

Microstructure and Mechanical Properties of Spark Plasma Sintered Amorphous $AlPO_4$ Ceramics

F. S. Sayyedan [a, *], M. H. Enayati [b], M. R. Rahimipour [c]

[a] *PhD, Department of Materials Engineering, Isfahan University of Technology (IUT), Isfahan, Isfahan, Iran*
[b] *Professor, Department of Materials Engineering, Isfahan University of Technology, Isfahan (IUT), Isfahan, Isfahan, Iran*
[c] *Professor, Department of Ceramics, Materials and Energy Research Center (MERC), Meshkindasht, Alborz, Iran*

* Corresponding Author Email: fs.sayyedan@alumni.iut.ac.ir (F. S. Sayyedan) URL: https://www.acerp.ir/article_145869.html

ARTICLE INFO

Article History:

Received 28 January 2022
Received in revised form 26 February 2022
Accepted 05 March 2022

Keywords:

Amorphous $AlPO_4$
Spark Plasma Sintering
Mechanical Properties
Fracture Toughness

ABSTRACT

The main objective of this study is to assess the structure and mechanical properties of amorphous aluminum phosphate ($AlPO_4$) ceramic specimens prepared through Spark Plasma Sintering (SPS) method. To this end, $AlPO_4$ powder was synthesized through sol-gel process and consolidated by SPS at the sintering temperature range of 800-1300 °C. Ceramic specimens were characterized by X-Ray Diffraction (XRD) and Scanning Electron Microscopy (SEM) analyses. Bulk density of the samples was measured using Archimedes' principle. In addition, hardness and indentation fracture toughness of the samples were determined to identify the mechanical properties. The results from XRD analysis, SEM images, and density measurement revealed that the sintered sample was characterized by an amorphous structure with the porosity of ~ 3 % and relative density of 97 % after SPS at 1000 °C for 15 min. Increasing the temperature to 1300 °C made the amorphous $AlPO_4$ crystallized. The fracture toughness was obtained to be 5.75 MPa.m$^{1/2}$ under this sintering condition. Crack deflection around porosities was identified as the main toughening mechanism involved.

https://doi.org/10.30501/ACP.2022.326779.1081

1. INTRODUCTION

High-Temperature Ceramic (HTC) materials mainly including high melting metal oxides, carbides, nitrides, and their composites are commonly used in a wide range of industrial applications such as metallurgy, cement, glass, aerospace, and energy [1]. HTCs are primarily applied owing to their thermal and thermo-mechanical properties. A number of studies have been and are still being conducted worldwide to find a novel class of HTCs characterized by preferential properties and develop the next generation of such materials. Some of their unique properties such as lightweight and low thermal conductivity make them excellent candidates to be applied in aerospace industries that are also highly demanded, thus yielding many superior and promising results [2].

Aluminum phosphate ($AlPO_4$) is a well-known ceramic material for its high melting point (1800 °C), high hardness (~ 1000 HV), low density (2.1-2.6 g.cm^{-3}), low electrical and thermal conductivities, and good corrosion and oxidation resistance at high-temperatures. This ceramic material can be widely used in the form of thin films, thick coatings, or bulk specimens in many applications, namely composites, catalysts, refractories, waterproof concrete, and phosphate-bonded ceramic

Please cite this article as: Sayyedan, F. S., Enayati, M. H., Rahimipour, M. R., "Microstructure and Mechanical Properties of Spark Plasma Sintered Amorphous $AlPO_4$ Ceramics", ***Advanced Ceramics Progress***, Vol. 7, No. 4, (2021), 52-58. https://doi.org/10.30501/ACP.2022.326779.1081

refractories, hence it can be regarded as one of the promising HTC materials [3].

Spark Plasma Sintering (SPS), also known as a rapid sintering method as well as a novel technique for synthesizing high-quality ceramic specimens, makes it feasible to maintain the intrinsic properties of powders in their fully dense products. Compared to conventional sintering methods such as Hot Pressing (HP) and Hot Isostatic Pressing (HIP), SPS process offers many advantages including easy operation, accurate control of sintering energy, high sintering speed followed by low grain growth, high reproducibility, safety, and reliability to name a few [4,5]. However, given the limitations of phase transformation, there are some restrictions in sintering the amorphous phases. Given that long sintering processes and high sintering temperatures may encourage crystallization, SPS process could be the right choice. Moreover, SPS makes it possible to obtain the maximum density at temperatures of at least 200 °C lower than those of HP or HIP [6]. For instance, Zhang et al. [7] fabricated transparent SiO_2 glass based on SPS at 900–1400 °C and reported the value of 98.5 % for the relative density of SiO_2 bodies at 1100 °C. They also employed Pressureless Sintering (PS) method to fabricate SiO_2 bodies for comparison and concluded that SPS was more effective than PS in terms of the depression of crystallization. SPS has also been used as a promising method to control the alumina microstructure by preventing the excessive grain growth during sintering due to the short holding times of only a few minutes. The main advantage of SPS was its ability to achieve densification without allowing excessive grain growth [8]. It can been used for sintering transparent ceramics, as discussed in a study by Apak et al. on the transparent polycrystalline alumina with optical properties identical to that of sapphire and Kanbur for transparent Aluminum OxyNitride (AlON) [9].

To the best of the authors' knowledge, no studies have been conducted on the fabrication of amorphous aluminum phosphate specimens using the SPS technique. In this regard, the present study primarily attempted to synthesize an amorphous $AlPO_4$ ceramic body based on SPS method and consider different process parameters to access desirable mechanical properties while preserving the initial amorphous structure.

2. MATERIALS AND METHODS

2.1. Amorphous $AlPO_4$ Powder Synthesis

Amorphous aluminum phosphate powder was synthesized through the sol-gel method, as explained in our previous report [10]. Table 1 gives the detailed characteristics of the precursors used to synthesize the starting powder. Aluminum nitrate nonahydrate and phosphorus pentoxide were separately dissolved in ethanol to achieve a clear solution with the molar ratio of Al/P:1.75/1. These two solutions were mixed together under agitation condition for two hours and let age at ambient temperature for 24 h. The prepared gel was dried in an oven at 150 °C in air to complete the dehydration process and get a voluminous and fluffy gel. The dried gel was calcined in an electrical furnace (Nobertherm N7/H, Germany) in air at 500 °C for 30 min to strengthen the gel structure and obtain the final powder product.

TABLE 1. Precursors used for synthesizing amorphous $AlPO_4$ powder

Composition	Chemical formula	Company	Purity (%)
Aluminum Nitrate Nonahydrate	$Al(NO_3)_3.9H_2O$	PENTA	98.5
Phosphorus Pentoxide	P_2O_5	PENTA	99.5
Ethanol	C_2H_5OH	PENTA	99.9

2.2. Spark Plasma Sintering

The prepared powder was sintered using SPS apparatus (SPS-20T-10, Easy Fashion, China) in a vacuum atmosphere considering the parameters listed in Table 2. The powder was poured into a die with the inner diameter of 15 mm and covered with graphite paper. The heating and cooling rate of 100 °C.min^{-1} and DC current pulse of 200/40:ms on/ms off were used for all samples. The graphite contaminations remaining from graphite foils on the sintered samples were eliminated using SiC sandpaper grinding wheel and polished using alumina slurry to 0.50 μm. In addition, X-Ray Diffractometer (XRD, Philips X'pert) was employed to carry out phase composition analysis of both starting powders and sintered specimens based on Cu Kα radiation (λ=1.54 Å, 40 kV, 30 mA) over the 2θ range of 10°–80°. Microstructural characterization was carried out on the polished surfaces of the sintered samples using Scanning Electron Microscopy (SEM, Philips XL30). The porosity of the specimens was assessed by ImageJ software.

TABLE 2. Parameters for sintering of amorphous $AlPO_4$ powder by SPS

Sample Number	Temperature (°C)	Holding Time (min)	Pressure (MPa)
1	800	30	50
2	900	20	50
3	1000	15	50
4	1300	10	50

2.3. Bulk and Relative Density Measurement

Bulk density (ρ_b, g.cm^{-3}) was measured in distilled water based on the ASTM B962-17 standard test method using Archimedes' principle and Equation (1) [11]:

$$\rho_b = \frac{A \times \rho_w}{B - C} \quad (1)$$

where A is the mass of the test piece in air (g), ρ_w the density of water (g.cm^{-3}), B the mass of the oil-impregnated test piece (g), and C the mass of the oil-impregnated test specimen in water with the mass of the specimen support tared (g). Finally, the relative density was measure using the ratio of the bulk density to the theoretical density.

2.4. Hardness and Fracture Toughness Evaluation

Hardness was also measured using a hardness testing machine (OTTO WOLPERT-WERKE GMBH, Germany) by Vickers indenter under a static load of 15 kg and at a dwell time of 10 s. The measurement was repeated five times to calculate the average value of the Vickers hardness (H_V) through Equation (2):

$$H_V = 1.85 \frac{f}{d^2} \quad (2)$$

where f is the load (kg), and d the average value of the two diagonals (mm).

Indentation fracture toughness was calculated from the length of the crack formed around the corners of indentations using the same hardness testing machine at a load of 20 kg. Fracture toughness (K_{IC}, MPa.m$^{1/2}$) was then calculated using both Equation (3) and Figure 1 [12]:

$$K_{IC} = 0.203\, H_V\, a^{1/2} \left(\frac{c}{a}\right)^{-3/2} \quad (3)$$

where H_V is the Vickers hardness (MPa), c the half length of the crack (m), and a the half length of the impression diagonal (m), as shown in Figure 1.

3. RESULTS AND DISCUSSION

The XRD patterns of aluminum phosphate powder calcined at 500 °C for 30 min accompanied with the spark plasma sintered specimens at different temperatures are illustrated in Figure 2. The results of the phase analysis of the powder confirmed the amorphous structure of $AlPO_4$ synthesized by the sol-gel process. The specimen sintered at 1000 °C for 15 min mainly preserved its amorphous structure. Sintering at 1300 °C for 10 min clearly transformed the structure from amorphous to crystalline by appearance of Al_2O_3 and $AlPO_4$ peaks.

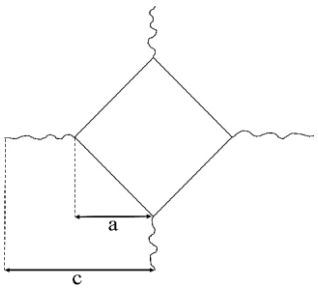

Figure 1. Schematic representation of crack generated by Vickers indenter

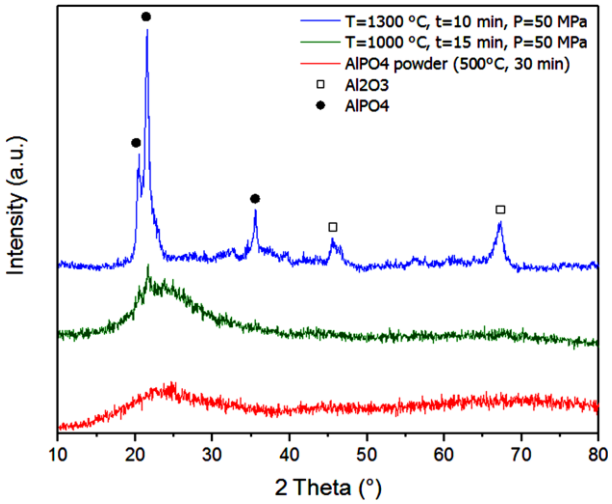

Figure 2. XRD patterns of $AlPO_4$ powder and spark plasma sintered specimens at different temperatures

Figure 3 depicts the SEM image and EDS analysis of $AlPO_4$ powder after annealing at 500 °C for 30 min. As observed in this figure, the average particle size of the powder used for the SPS process was less than 10 µm. Furthermore, the EDS analysis of $AlPO_4$ powder confirmed the presence of Al, P, and O elements in the powder structure.

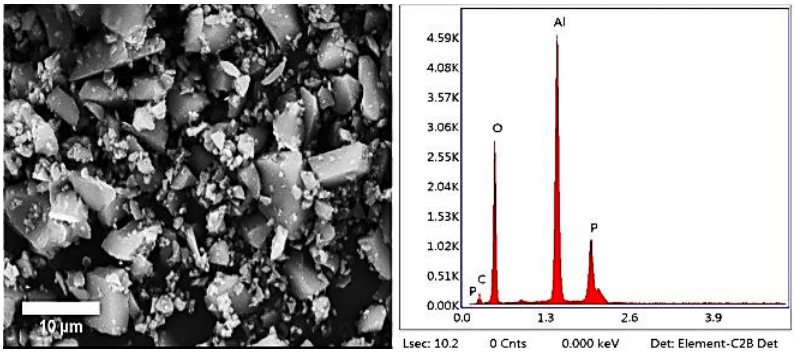

Figure 3. SEM image and EDS analysis of $AlPO_4$ powder after annealing at 500 °C for 30 min

Figure 4 shows the SEM images of the spark plasma sintered specimens processed under pressure of 50 MPa at different temperatures and different holding times. As shown in Figure 4a and Figure 4b, the temperatures of 800 °C and 900 °C were not sufficient to make dense $AlPO_4$ specimens. As a result, some irregular particles are observed in these images that are stuck together. According to Figure 4c, the consolidation process was completed upon increasing the sintering temperature to 1000 °C. However, a fully dense and porosity-free specimen was not formed. As shown in Figure 4d, further increase in the temperature to 1300 °C did not help reduce porosities.

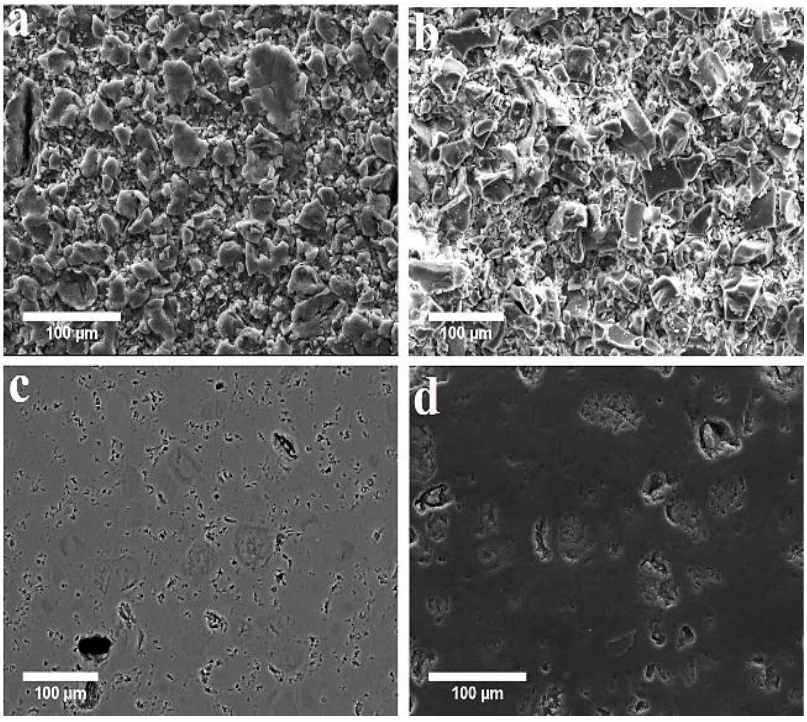

Figure 4. SEM images of spark plasma sintered specimens under pressure of 50 MPa at (a) 800 °C for 30 min, (b) 900 °C for 20 min, (c) 1000 °C for 15 min, and (d) 1300 °C for 10 min

Figure 5 presents the image analysis results using ImageJ software, and Table 3 shows the porosity values of 3 % and 1.5 % with the average porosity sizes of 3 µm and 2 µm for the samples sintered at 1000 °C for 15 min (Figures 5a and 5b) and 1300 °C for 10 min (Figures 5c and 5d), respectively. Table 3 also indicates that the values of the relative density of the samples sintered at 1000 °C for 15 min and 1300 °C for 10 min were 97 % and 98.5 %, respectively. Of note, a theoretical density of 2.2 $g.cm^{-3}$ was used for calculating the relative density. While increasing the sintering temperature to 1300 °C produced a slightly more compact specimen than that produced at 1000 °C, the microstructure of the sintered sample at 1300 °C did not exhibit significant changes compared to the one sintered at 1000 °C (see Figure 5). However, the structure transition from amorphous to crystalline occurred at temperatures over 1000 °C according to the XRD patterns presented in Figure 2. In this respect, the sample sintered at 1000 °C for 15 min was selected for the next measurement mechanical properties.

Figure 6 presents the diagonal of the Vickers indentation for the sintered specimen at 1000 °C for 15 min under a load of 15 kg at the dwell time of 10 s. The value of the Vickers hardness (H_V) was calculated as 2104 MPa based on Equation (2).

Figure 7 shows the indentation crack propagation path in the specimen sintered at 1000 °C for 15 min. The fracture toughness of this sample was calculated as 5.75 $MPa.m^{1/2}$ based on Equation (3) which can be a significant amount among the monolithic ceramic compacts. As observed in Figure 7b, the crack deflection around the micropores was the dominant toughening mechanism involved. Crack deflection accompanied with a significant stress relaxation at the tip of the crack near porosities suppressed the crack propagation and enhanced the fracture toughness [13]. The idea that lies behind all toughening mechanisms in monolithic ceramics is to increase the energy required for crack propagation [14]. Accordingly, four main toughening mechanisms were introduced: crack deflection [15], crack bridging [16], crack branching [17], and microcracking [18]. Porous ceramics exhibit several

advantages, in particular, lower thermal conductivity and strong thermal shock resistance, lighter weight, and higher fracture toughness [19-21] than those of their dense counterparts.

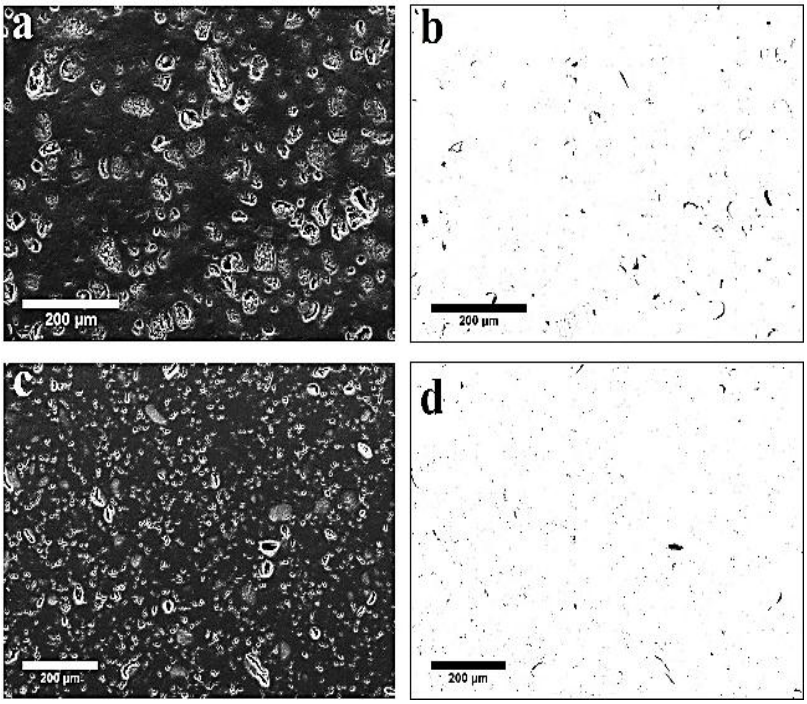

Figure 5. Porosity analysis by ImageJ software for SEM images of the spark plasma sintered specimens at the pressure of 50 MPa and (a,b) 1000 °C for 15 min and (c,d) 1300 °C for 10 min

TABLE 3. Porosity, bulk, and relative density of the sintered specimens based on the SPS process

Sample number	Porosity (%)	Porosity size (µm)	Bulk density ($g.cm^{-3}$)	Relative density (%)
3	3	15±3	2.1	97.0
4	1.5	12±2	2.2	98.5

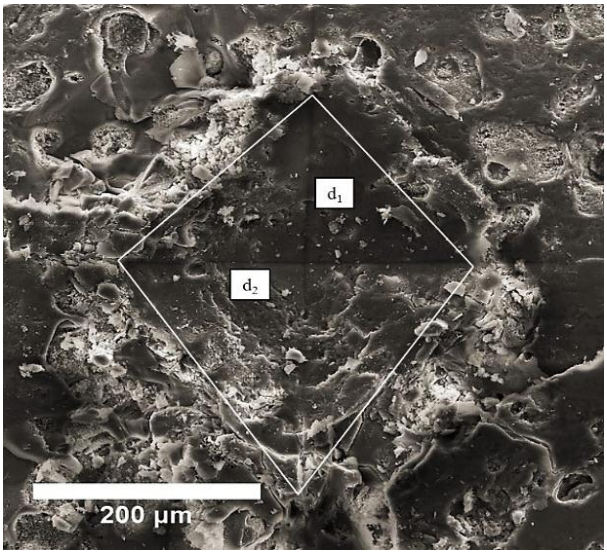

Figure 6. Vickers indentation at a load of 15 kg and a dwell time of 10 s

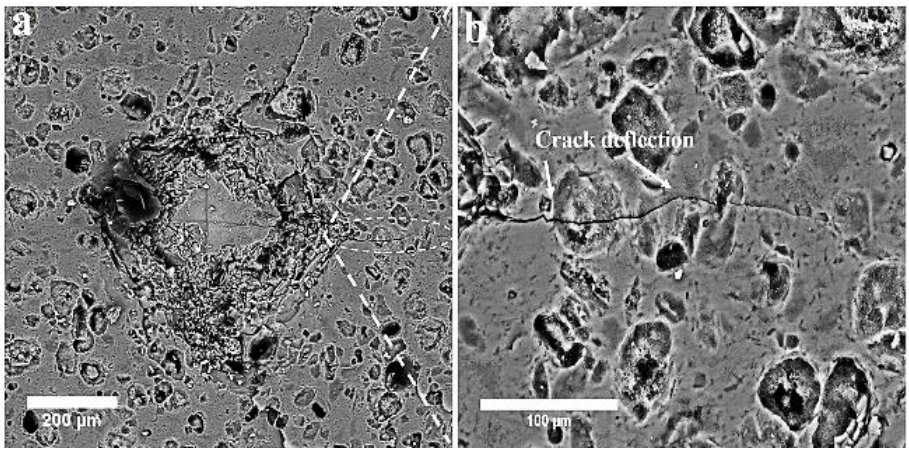

Figure 7. (a) Vickers indentation at a load of 20 kg and a dwell time of 10 s and (b) Crack propagation path demonstrating the toughening mechanism of crack deflection

Ghahremani et al. [22] evaluated the effects of the SPS parameters including the sintering temperature, applied pressure, and dwell time on the mechanical properties of the densified mullite specimens. They concluded that an increase in the applied pressure and dwell time would increase the density of the mullite. They reported the temperature of 1700 °C, dwell time of 15 min, and applied pressure of 20 MPa as the optimum parameters to obtain a relative density of 99 % and fracture toughness of 2.8 MPa.$m^{1/2}$. In addition, the maximum fracture toughness of 4 MPa.$m^{1/2}$ was obtained while decreasing the relative density to 95.5 %. They declared that in fully-dense compacts, the crack was propagated in a straight-line path. On the contrary, in the case of porous compacts, the crack moved through a non-straight route due to the crack tip deflection at the pores which required more energy to propagate.

Lu et al. [23] fabricated porous Si_3N_4 ceramics by die pressing at 1800-1900 °C for four hours and subsequently, gel casting and gas-pressure sintering were performed to obtain high-porosity Si_3N_4 specimens. Their results showed that the sample with 37 % porosity was characterized by a higher fracture toughness value (3.53 MPa.$m^{1/2}$) than that with 32 % porosity (2.11 MPa.$m^{1/2}$). They attributed this behavior to the role of pores as the crack arresters and suggested a scenario to elaborate the toughening mechanism. They declared that followed by encountering a crack to a pore, the crack would be constrained to alter its path or stop at the pore. In this situation, the cracks propagated over a shorter distance, and they would be arrested by the pores, thus resulting in an increase in the crack resistance against growth in high porous ceramics.

Crack deflection and bridging could also occur around grain boundaries in polycrystalline materials and second-phase particles in composite specimens [13]. He et al. [24] studied the mechanical properties of nano-grain SiO_2 glass prepared through SPS process. A relative density of above 90 % was obtained in the sintering temperature range of 1300–1550 °C. The SiO_2 specimen exhibited the highest hardness and fracture toughness of 14.2 GPa and 5.4 MPa.$m^{1/2}$ at the optimum sintering temperature of 1450 °C, respectively. They concluded that the microstructure with nano-grain SiO_2 glass was responsible for crack deflection and high K_{IC} value. G. M. Asmelash et al. [25] evaluated the fracture toughness of Al_2O_3–SiO_2–ZrO_2 composite materials prepared by PS. The fracture toughness of the composite containing 75 wt. % Al_2O_3–10 wt. % SiO_2–15 wt. % ZrO_2 was reported to be 2.39 MPa.$m^{1/2}$. They realized that reinforcement particles (SiO_2+ZrO_2) in the alumina matrix played a key role in toughening, considering three toughening mechanisms namely crack deflection, crack bridging, and microcracks.

4. CONCLUSION

$AlPO_4$ ceramic specimens were fabricated through SPS process at the sintering temperature range of 800-1300 °C. In addition, the microstructure and mechanical properties including hardness and fracture toughness were characterized in this study. The obtained results revealed that the temperatures below 1000 °C were not sufficient to reach a dense specimen, while sintering at temperatures above 1000 °C clearly transformed the amorphous structure into the crystalline state. The sample sintered at 1000 °C for 15 min retained its initial amorphous structure with the relative density of 97 % and porosity of 3 %. The fracture toughness for this sample was 5.75 MPa.$m^{1/2}$ which could be a considerable value compared to those reported for other monolithic ceramics. Microstructural examination of the cracked surface revealed that crack deflection around micropores was the main toughening mechanism involved.

ACKNOWLEDGEMENT

The authors acknowledge the support of Department of Materials Engineering, Isfahan University of Technology and Ceramics Department of Materials and Energy Research Center in this research.

REFERENCES

1. Zhang, S., "High temperature ceramic materials", ***Materials***, Vol. 14, No. 8, (2021), 2031. https://doi.org/10.3390/ma14082031
2. He, J., Li, X., Su, D., Ji, H., Wang, X., "Ultra-low thermal conductivity and high strength of aerogels/fibrous ceramic composites", ***Journal of the European Ceramic Society***, Vol. 36, No. 6, (2016), 1487-1493. https://doi.org/10.1016/j.jeurceramsoc.2015.11.021
3. Sayyedan, F. S., Enayati, M. H., "On structure and oxidation behaviour of non-stoichiometric amorphous aluminium phosphate coating", ***Surface Engineering***, Vol. 35, No. 8, (2019), 670-676. https://doi.org/10.1080/02670844.2018.1560912
4. Anselmi-Tamburini, U., "Spark plasma sintering", ***Encyclopedia of Materials: Technical Ceramics and Glasses***, Vol. 1, (2021), 294-310. https://doi.org/10.1016/B978-0-12-803581-8.11730-8
5. Kermani, M., Razavi, M., Rahimipour, M. R., Zakeri, M., "The effect of temperature on the in situ synthesis–sintering and mechanical properties of $MoSi_2$ prepared by spark plasma sintering", ***Journal of Alloys and Compounds***, Vol. 585, (2014), 229-233. https://doi.org/10.1016/j.jallcom.2013.09.125
6. Hong, J., Gao, L., Torre, S. D. D. L., Miyamoto, H., Miyamoto, K., "Spark plasma sintering and mechanical properties of $ZrO_2(Y_2O_3)$–Al_2O_3 composites", ***Materials Letters***, Vol. 43, No. 1-2, (2000), 27-31. https://doi.org/10.1016/S0167-577X(99)00225-6
7. Zhang, J., Tu, R., Goto, T., "Fabrication of transparent SiO_2 glass by pressureless sintering and spark plasma sintering", ***Ceramics International***, Vol. 38, No. 4, (2012), 2673-2678. https://doi.org/10.1016/j.ceramint.2011.11.034
8. Mansoor, M., Mansoor, M., Mansoor, M., Er, Z., Çinar Şahin, F., "Ab-initio study of paramagnetic defects in Mn and Cr doped transparent polycrystalline Al_2O_3 ceramics", ***Synthesis and Sintering***, Vol. 1, No. 3, (2021), 135-142. https://doi.org/10.53063/synsint.2021.1340
9. Mansoor, M., Mansoor, M., Mansoor, M., Themelis, T., Çinar Şahin, F., "Sintered transparent polycrystalline ceramics: the next generation of fillers for clarity enhancement in corundum", ***Synthesis and Sintering***, Vol. 1, No. 3, (2021), 183-188. https://doi.org/10.53063/synsint.2021.1342
10. Sayyedan, F. S., Enayati, M. H., Hashempour, M., Vicenzo, A., Bestetti, M., "Synthesis and characterization of sol-gel derived non-stoichiometric aluminum phosphate coating", ***Surface and Coatings Technology***, Vol. 351, (2018), 128-135. https://doi.org/10.1016/j.surfcoat.2018.07.086
11. Bassett, K., Carriveau, R., Ting, D. S. K., "Underwater energy storage through application of Archimedes principle", ***Journal of Energy Storage***, Vol. 8, (2016), 185-192. https://doi.org/10.1016/j.est.2016.07.005
12. Tekeli, S., "Fracture toughness (K_{IC}), hardness, sintering and grain growth behaviour of 8YSCZ/Al_2O_3 composites produced by colloidal processing", ***Journal of Alloys and Compounds***, Vol. 391, No. 1-2, (2005), 217-224. https://doi.org/10.1016/j.jallcom.2004.08.084
13. Launey, M. E., Ritchie, R. O., "On the fracture toughness of advanced materials", ***Advanced Materials***, Vol. 21, No. 20, (2009), 2103-2110. https://doi.org/10.1002/adma.200803322
14. Launey, M. E., Munch, E., Alsem, D. H., Barth, H. B., Saiz, E., Tomsia, A. P., Ritchie, R. O., "Designing highly toughened hybrid composites through nature-inspired hierarchical complexity", ***Acta Materialia***, Vol. 57, No. 10, (2009), 2919-2932. https://doi.org/10.1016/j.actamat.2009.03.003
15. Awaji, H., Ebisudani, M., Choi, S. M., Ohashi, T., "Crack Deflection Toughening mechanism in brittle materials", In ***Fracture Resistance Testing of Monolithic and Composite Brittle Materials***, ASTM International, West Conshohocken, PA, USA, (2009), 137-151. https://doi.org/10.1520/STP10476S
16. Erdogan, F., Joseph, P. F., "Toughening of ceramics through crack bridging by ductile particles", ***Journal of the American Ceramic Society***, Vol. 72, No. 2, (1989), 262-270. https://doi.org/10.1111/j.1151-2916.1989.tb06112.x
17. Bleyer, J., Roux-Langlois, C., Molinari, J. F., "Dynamic crack propagation with a variational phase-field model: limiting speed, crack branching and velocity-toughening mechanisms", ***International Journal of Fracture***, Vol. 204, No. 1, (2017), 79-100. https://doi.org/10.1007/s10704-016-0163-1
18. Ohji, T., Jeong, Y. K., Choa, Y. H., Niihara, K., "Strengthening and toughening mechanisms of ceramic nanocomposites", ***Journal of the American Ceramic Society***, Vo. 81, No. 6, (1998), 1453-1460. https://doi.org/10.1111/j.1151-2916.1998.tb02503.x
19. Chen, Y., Wang, N., Ola, O., Xia, Y., Zhu, Y., "Porous ceramics: Light in weight but heavy in energy and environment technologies", ***Materials Science and Engineering: R: Reports***, Vol. 143, (2021), 100589. https://doi.org/10.1016/j.mser.2020.100589
20. Li, Y., Wu, H., Liu, X., Huang, Z., "Microstructures and properties of porous liquid-phase-sintered SiC ceramic by hot press sintering", ***Materials***, Vol. 12, No. 4, (2019), 639. https://doi.org/10.3390/ma12040639
21. Jin, X., Dong, L., Xu, H., Liu, L., Li, N., Zhang, X., Han, J., "Effects of porosity and pore size on mechanical and thermal properties as well as thermal shock fracture resistance of porous ZrB_2–SiC ceramics", ***Ceramics International***, Vol. 42, No. 7, (2016), 9051-9057. https://doi.org/10.1016/j.ceramint.2016.02.164
22. Ghahremani, D., Ebadzadeh, T., Maghsodipour, A., "Spark plasma sintering of mullite: Relation between microstructure, properties and spark plasma sintering (SPS) parameters", ***Ceramics International***, Vol. 41, No. 5, (2015), 6409-6416. https://doi.org/10.1016/j.ceramint.2015.01.078
23. Lu, X., Wei, Y., Wang, H., Wen, J., Zhou, J., Fan, J., "Porosity and oxide layer dependence of thermal shock behavior of porous silicon nitride ceramics", ***Journal of Materials Science & Technology***, Vol. 30, No. 12, (2014), 1217-1222. https://doi.org/10.1016/j.jmst.2014.11.004
24. He, Z., Katsui, H., Goto, T., "Mechanical properties of nano-grain SiO_2 glass prepared by spark plasma sintering", ***Journal of the European Ceramic Society***, Vol. 37, No. 2, (2017), 721-725. https://doi.org/10.1016/j.jeurceramsoc.2016.09.020
25. Asmelash, G. M., Mamat, O., Ahmad, F., "Toughening mechanisms of Al_2O_3–SiO_2–ZrO_2 composite materials", ***Ceramics-Silikáty***, Vol. 56, No. 4, (2012). 360-366. https://www.irsm.cas.cz/materialy/cs_content/2012/Asmelash_CS_2012_0000.pdf